Blue HLCT fluorophore for high-performance and color stable white OLEDs via balanced bipolar transport

Jiankang Deng(邓建康), Qiao Luo(罗巧), Chunming Xiong(熊春明), Lixiao Luo(罗力潇), Xin Ge(葛鑫), Ding Zheng(郑丁), Junsheng Yu(于军胜)

Citation: Chin. Phys. B. 35, 107804 (2026). DOI: 10.1088/1674-1056/ae1f01 | CSTR: 32038.14.CPB.ae1f01
http://cpb.iphy.ac.cn; http://iopscience.iop.org/cpb

What follows is a list of articles you may be interested in

Improvement of electro-optic performances in white organic light emitting diodes with color stability by buffer layer and multiple dopants structure

Zhi-Qi Kou(寇志起), Yu Tang(唐宇), Li-Ping Yang(杨丽萍), Fei-Yu Yang(杨飞宇), Wen-Jun Guo(郭文军)
Chin. Phys. B. 27, 107801 (2018). DOI: 10.1088/1674-1056/27/10/107801

High color rendering index white organic light-emitting diode using levofloxacin as blue emitter

Miao Yan-Qin(苗艳勤), Gao Zhi-Xiang(高志翔), Zhang Ai-Qin(张爱琴), Li Yuan-Hao(李源浩), Wang Hua(王华), Jia Hu-Sheng(贾虎生), Liu Xu-Guang(刘旭光), Tsuboi Taiju
Chin. Phys. B. 24, 057802 (2015). DOI: 10.1088/1674-1056/24/5/057802

Tandem white organic light-emitting diodes adopting a C_{60}: rubrene charge generation layer

Bi Wen-Tao(毕文涛), Wu Xiao-Ming(吴晓明), Hua Yu-Lin(华玉林), Sun Jin-E(孙金娥), Xiao Zhi-Hui(肖志慧), Wang Li(王丽), Yin Shou-Gen(印寿根)
Chin. Phys. B. 23, 017803 (2014). DOI: 10.1088/1674-1056/23/1/017803

Photoluminescence in transition metal dichalcogenides: Towards high quantum yield

Xin Yan(闫欣), Weijia Tang(汤唯佳), Guilong Gao(高贵龙), Kai He(何凯), Dong Yao(姚东), Butian Zhang(张卜天), Shun Wang(王顺), Youwei Zhang(张有为)
Chin. Phys. B. 35, 087801 (2026). DOI: 10.1088/1674-1056/ae60f1 | CSTR: 32038.14.CPB.ae60f1

Blue–green luminescence properties and energy transfer in Tm^{3+}/Tb^{3+} co-doped TeO_2–GeO_2–Bi_2O_3–BaF_2 glass

Ruizhen Pang(庞瑞祯), Tong Wu(吴童), Kexuan Han(韩科选), Zhenyu Zhou(周振宇), Wei Zheng(郑威)
Chin. Phys. B. 35, 077801 (2026). DOI: 10.1088/1674-1056/ae12d0 | CSTR: 32038.14.CPB.ae12d0

Blue HLCT fluorophore for high-performance and color stable white OLEDs via balanced bipolar transport

Jiankang Deng(邓建康), Qiao Luo(罗巧), Chunming Xiong(熊春明),
Lixiao Luo(罗力潇), Xin Ge(葛鑫), Ding Zheng(郑丁)†, and Junsheng Yu(于军胜)‡

State Key Laboratory of Electronic Thin Films and Integrated Devices, School of Optoelectronic Science and Engineering, University of Electronic Science and Technology of China (UESTC), Chengdu 610054, *China*

(Received 12 September 2025; revised manuscript received 7 November 2025; accepted manuscript online 13 November 2025)

White organic light-emitting diodes (OLEDs) hold a highly significant position in the fields of display and lighting. However, achieving both high efficiency and color stability in white OLEDs remains a persistent challenge. The recently developed hybridized local and charge transfer (HLCT) material PPIAn2N maximizes exciton utilization due to the bipolar nature of its PPI units and the efficient reverse intersystem crossing (RISC) from high-lying triplet states (T_n, $n \geq 2$) to the singlet state (S_1), suggesting its great potential for constructing high-performance white OLEDs. In this work, the blue HLCT material PPIAn2N is employed as a sensitizing host to fabricate red fluorescent and yellow phosphorescent OLEDs based on DCJTB and PO-01, respectively, by precise concentration control. The resulting devices achieve maximum external quantum efficiencies (EQEs) of 6.88% and 25.08%. Notably, the red device surpasses the theoretical EQE limit of 5% for conventional fluorescent OLEDs, and the yellow device exhibits negligible efficiency roll-off. Building upon this, a strategically designed dual-emission layer architecture enables PPIAn2N, with its bipolar carrier transport property, to function simultaneously as a blue emitter and as a sensitizing host for PO-01 in hybrid fluorescence/phosphorescence white OLEDs. The resulting device exhibits a maximum EQE of 17.03% and a maximum luminance of 74098 cd/m^2. Furthermore, a stable electroluminescence (EL) spectrum is maintained over a wide voltage range. We believe this work provides a new strategy for the development of high-performance doped monochromatic and color-stable white OLEDs.

Keywords: white OLEDs, hybridized local and charge transfer (HLCT) material, high-performance, balanced bipolar transport

PACS: 78.60.Fi, 85.60.Jb, 81.05.Fb

DOI: 10.1088/1674-1056/ae1f01 **CSTR:** 32038.14.CPB.ae1f01

1. Introduction

In recent years, organic light-emitting diodes (OLEDs) have become an indispensable part of modern life due to their advantages such as self-emission, fast response, high color quality, and flexibility.[1–4] White OLEDs are a pivotal branch of OLEDs and show great promise for applications in full-color displays and commercial lighting.[5,6] Among the components of white OLEDs, blue emitters are particularly critical, as they not only serve as one of the three primary colors but also function as host materials to enable green, red, and white emissions through energy transfer to longer-wavelength dopants.[7–9] Moreover, blue emitters play a vital role in reducing power consumption and achieving high color gamut and resolution in display and lighting applications.[10–12] The lack of efficient and stable blue emitters has become a major bottleneck in the advancement of high-performance monochromatic and white OLEDs. Traditional fluorescent materials are fundamentally limited by the 5% theoretical upper limit of EQE, where merely 25% of singlet excitons are utilized for light emission.[13,14] Phosphorescent OLEDs also typically suffer from severe efficiency roll-off, leading to short operating lifetimes at practical luminance levels.[15] Moreover, the scarcity of stable blue phosphorescent materials critically hinders the development of all-phosphorescent white OLEDs.[16,17] The intrinsically long exciton lifetimes of thermally activated delayed fluorescence (TADF) materials lead to pronounced efficiency roll-off and short device lifetimes, posing new bottlenecks.[18] Recently, OLED materials based on the "hot exciton" mechanism have advanced rapidly. These materials feature dual excited-state components, charge transfer (CT) and localized excitation (LE), demonstrating practical advantages in utilizing both singlet and triplet excitons.[19,20] This mechanism helps mitigate efficiency roll-off caused by triplet excitons in non-doped OLEDs. In addition, in doped OLEDs, the high efficiency roll-off of TADF materials as sensitizing hosts is a critical issue, as the long exciton lifetime leads to an increase in exciton concentration with increasing brightness. This, in turn, raises the probability of molecular degradation processes, resulting in energy loss. To date, monochromatic OLEDs employing HLCT materials have achieved both high EQE and low efficiency roll-off.[19–24]

†Corresponding author. E-mail: dingzheng@uestc.edu.cn
‡Corresponding author. E-mail: jsyu@uestc.edu.cn

© 2026 Chinese Physical Society and IOP Publishing Ltd. All rights, including for text and data mining, AI training, and similar technologies, are reserved.

Host–guest doping serves as an effective and widely employed approach to improve the electroluminescent (EL) performance of doped OLEDs. To maintain effective energy transfer from host to guest in the emissive layer, an ideal host material should possess the following characteristics: (i) higher singlet and triplet energy levels than the guest material to ensure complete energy transfer and confine excitons on the guest,[25] (ii) appropriate highest occupied molecular orbital (HOMO) and lowest unoccupied molecular orbital (LUMO) levels to promote carrier injection into the emissive layer,[10] (iii) excellent bipolar carrier transport property to maintain balanced carrier injection/transport, where broadening the recombination zone facilitates exciton generation and recombination,[26] and (iv) good thermal and morphological stability. Recent studies have demonstrated that blue HLCT materials can serve as host materials for both fluorescent and phosphorescent emitters, enabling high-efficiency and low roll-off monochromatic and white OLEDs through energy transfer strategies.[27–29] In 2023, Yang *et al*. employed the HLCT blue emitter PAC as a sensitizer for the traditional blue fluorescent molecule DSA-ph to enhance the performance of conventional blue fluorescent OLEDs. The resulting device exhibited efficient blue emission with a maximum EQE of 6.2%.[27] In 2024, Liu *et al*. developed two HLCT blue materials, PPyIM and PPIM. PPyIM was used as a non-doped blue emitting layer, while a PPIM/PO-01 combination served as the orange-emitting layer. The resulting dual-emission hybrid WOLED achieved an excellent EQE of 26.5% and with a remarkably stable color over a practical brightness range of 400 to 10000 cd/m^2, showing a CIE coordinate shift as small as (0.004, 0.003).[28] In 2024, Li *et al*. employed pCzAnN simultaneously as a blue emitter and as a sensitizing host for the fluorescent dopants C545T and DCJTB, realizing a fully fluorescent three-color white OLED. All three-color white devices showed negligible roll-off ($< 1\%$ at 1000 cd/m^2) and a high color rendering index (CRI) of 87.[29]

In the present paper, the bipolar transport property of the blue hybridized local and charge transfer material PPIAn2N is employed as a sensitizing host material. By precisely controlling the doping concentration, red fluorescent and yellow phosphorescent OLEDs based on DCJTB ((4-(dicyanomethylene)-2-tert-butyl-6-(1,1,7,7-tetramethyljulolidin-4-yl-vinyl)-4H-pyran) and PO-01 (2-(thieno[3,2-c]pyridin-4-yl)phenyl]iridium(III)) are fabricated, achieving maximum EQEs of 6.88% and 25.08%. Building on this, a strategically designed dual-emission layer structure is developed, in which PPIAn2N serves simultaneously as the blue emitter and the sensitizing host for PO-01 in a hybrid fluorescence/phosphorescence white OLED. The resulting device exhibits a maximum current efficiency (CE) of 38.67 cd/A, a maximum power efficiency (PE) of 39.90 lm/W, a maximum EQE of 17.03%, and a maximum luminance of 74098 cd/m^2. A stable EL spectrum is maintained over a wide voltage range, highlighting its great potential for practical applications.

2. Results and discussion

Recently, our group reported a blue hot exciton material PPIAn2N with HLCT characteristics, achieving notable EL performance including a 452-nm emission peak and a 7.3% maximum EQE as shown in Fig. 1(a). In addition, its LUMO and HOMO are -2.55 eV and -5.55 eV, respectively, and it exhibits strong absorption in the ultraviolet region. Crucially, PPIAn2N exhibits a typical bipolar carrier transport property with hole/electron mobilities of 4.75×10^{-6} cm$^2\cdot$V$^{-1}\cdot$s^{-1} and 1.70×10^{-7} cm$^2\cdot$V$^{-1}\cdot$s^{-1}.[22] The low-temperature phosphorescence spectrum of PPIAn2N at 77 K is shown in the supporting information Fig. S1, and the corresponding T_1 is 2.35 eV. The above results reveal great potential for fabricating high-performance doped OLEDs.

The molecular structures of the red fluorescent emitter DCJTB and the yellow phosphorescent emitter PO-01 are displayed in Fig. 1(b). The molecular structures of other materials involved in this work are provided in Fig. S2. Prior to device fabrication, the photophysical properties of the three emitters were investigated. It is evident from Fig. 1(c) that the photoluminescence (PL) spectrum of PPIAn2N exhibits significant spectral overlap with the UV–Vis absorption spectra of both DCJTB and PO-01, indicating the feasibility of Förster energy transfer (FRET) from PPIAn2N to DCJTB or PO-01.[30] The PL spectra of films doped with 0.8-wt% DCJTB and 8-wt% PO-01 in PPIAn2N are depicted in Fig. 1(d), from which it can be seen that a very weak emission peak appears at 448 nm and a main emission peak is observed at 608 nm in the PPIAn2N:DCJTB co-doped film. For the PPIAn2N:PO-01 co-doped film, two emission peaks of nearly equal intensity are observed at 448 nm and 595 nm. These major emission peaks correspond to the intrinsic emissions of DCJTB and PO-01, respectively, confirming the occurrence of energy transfer from PPIAn2N to the guest emitters. The shortwave emission observed in the doped films (peak at 448 nm) is attributed to incomplete energy transfer from the PPIAn2N host. These results provide preliminary evidence for the feasibility of employing PPIAn2N as a host material in doped OLEDs.

Based on the above analysis, a series of red fluorescent OLEDs are fabricated by doping the fluorescent material DCJTB in PPIAn2N, experimentally validating the feasibility of PPIAn2N as a fluorescent host. The detailed device configuration is indium tin oxide (ITO)/MoO_3 (3 nm)/TAPC (40 nm)/TCTA (10 nm)/PPIAn2N: DCJTB (x wt%, 10 nm)/TmPyPB (40 nm)/LiF (1 nm)/Al (100 nm) ($x = 0.5$, 0.8, and 1.0 correspond to devices R1, R2, and R3). As is well known, FRET is a long-range energy transfer process, and efficient energy transfer from the host ma-

terial to the fluorescent dopant can be achieved by controlling the doping concentration within 2 wt%.[31] According to previous studies, efficient energy transfer and optimal device performance in DCJTB-doped OLEDs typically occur when the doping concentration is maintained below 1.0%, as higher concentrations often lead to concentration quenching and reduced emission efficiency.[29] Different doping concentrations are employed to manipulate the energy transfer process from PPIAn2N to DCJTB, aiming to optimize EL performance. In this structure, ITO and Al serve as the anode and cathode, respectively; MoO_3 and LiF act as the hole and electron injection layers; 4,4'-Cyclohexylidenebis [N, N-bis(p-tolyl)aniline] (TAPC) is the hole-transporting layer; tris(4-carbazoyl-9-ylphenyl)amine (TCTA) serves as the exciton blocking layer (EBL); PPIAn2N: DCJTB is the emitting layer (EML) and 1,3,5-tri[(3-pyridyl)phen-3-yl]benzene (TmPyPB) is used as the electron-transporting layer (ETL). The detailed structure and energy-level diagram are depicted in Fig. 2(a).

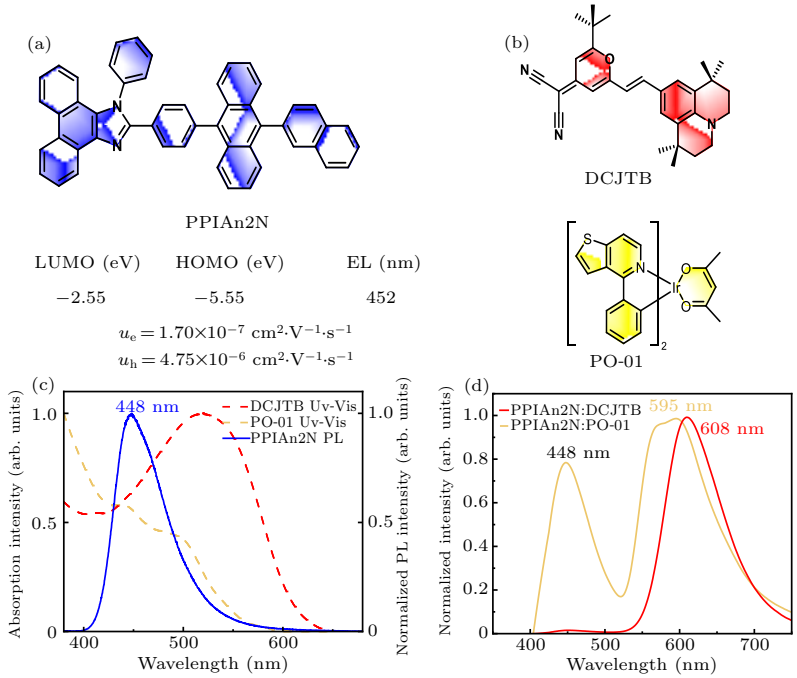

Fig. 1. (a) Schematic diagram of the molecular structure and properties of PPIAn2N, (b) molecular structures of DCJTB and PO-01, (c) UV–vis absorption spectra of DCJTB/PO-01 and normalized PL spectra of PPIAn2N in neat film, (d) normalized PL spectra of PPIAn2N:0.8-wt% DCJTB and PPIAn2N:8-wt% PO-01 films.

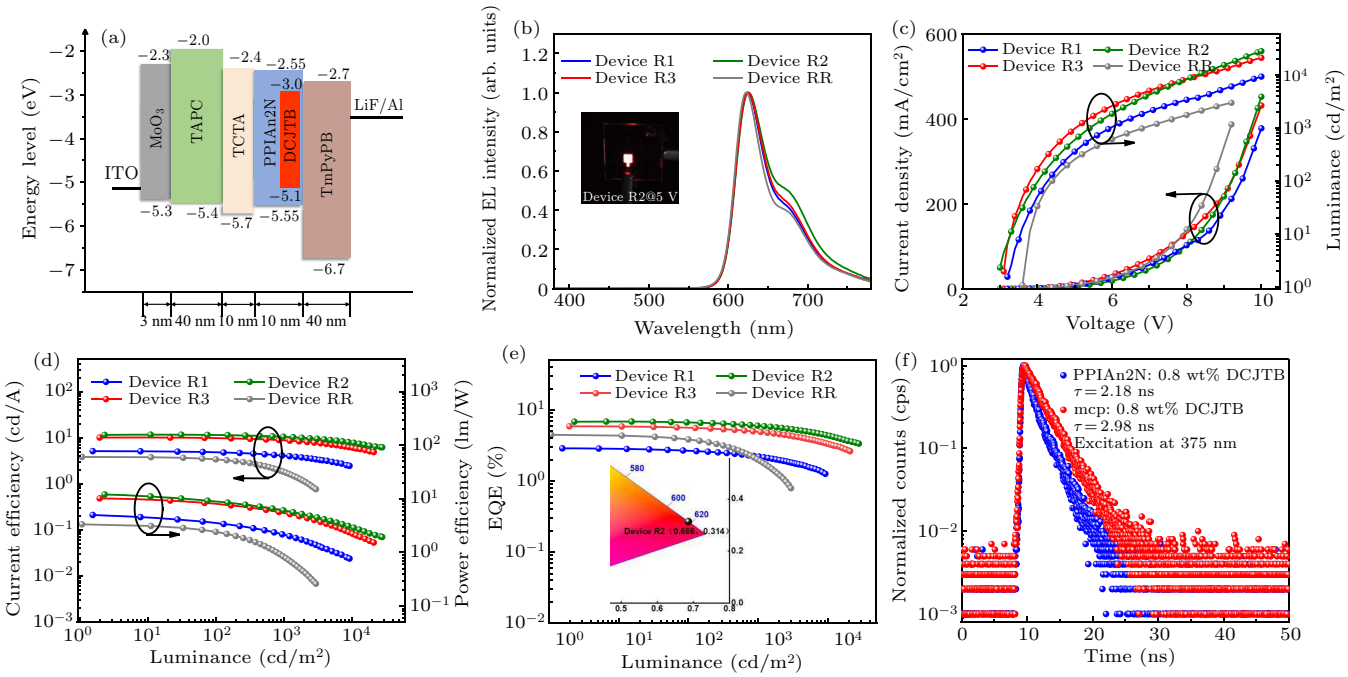

Fig. 2. (a) Schematic device structure and energy level diagram for red devices, (b) normalized EL spectra for red devices at 5 V, (c) current density–voltage–luminance (*J*–*V*–*L*) curves; (d) current efficiency–luminance–power efficiency (CE–L–PE) curves, (e) EQE—luminance (EQE–L) curves and CIE coordinates of R2 device at 5 V, (f) transient PL decay curves of PPIAn2N:0.8-wt% DCJTB and mCP:0.8-wt% DCJTB films.

Table 1. Summary of key performance parameters for red and yellow devices in this work.

Device	V_{on} (V)	L_{max} (cd/m^2)	CE (cd/A)/PE (lm/W)/EQE (%)		CIE(x,y)	Roll off (%)
			Maximum	At 1000 cd/m^2		
R1	3.2	9242	5.11/5.01/2.89	4.06/2.12/2.21	(0.684,0.315)	23.5
R2	3.0	27982	11.64/12.04/6.88	10.49/6.10/6.02	(0.686,0.314)	12.5
R3	3.1	21008	10.08/10.20/5.89	8.78/5.52/4.96	(0.685,0.315)	15.8
RR	3.6	2965	3.83/3.35/4.48	1.84/0.85/2.03	(0.677,0.319)	54.7
Y1	2.4	55422	49.45/56.89/16.82	49.37/53.48/16.70	(0.526,0.462)	0.7
Y2	2.4	93975	63.65/72.38/25.08	63.59/66.59/25.03	(0.533,0.459)	0.2
Y3	2.4	77279	62.21/71.30/21.99	61.49/62.32/21.10	(0.537,0.457)	4.0

V_{on}: the voltage at the luminance of 1 cd/m^2; L_{max}: the maximum luminance of the devices; CIE(x,y): CIE coordinates obtained at a voltage of 5 V; Roll off: roll off value = (maximum EQE – EQE@1000 cd/m^2)/maximum EQE.

As shown in the EL spectra in Figs. 2(b) and S3, devices R1–R3 exhibit red emission with a peak located at 625 nm, corresponding to the intrinsic emission of DCJTB.[32] As displayed in Fig. 2(c), the turn-on voltages of devices R1–R3 range from 3.0 V to 3.2 V, which can be attributed to the well-aligned energy levels for hole and electron injection as illustrated in Fig. 2(a). The EL performance of devices R1–R3 is closely correlated with the doping concentration of DCJTB. As the doping concentration increases, the device performance first improves and then declines (Figs. 2(c)–2(e)). For example, the maximum luminance, CE, PE, and EQE of device R1 are 9242 cd/m^2, 5.11 cd/A, 5.01 lm/W, and 2.89%, respectively; those of device R2 are 27982 cd/m^2, 11.64 cd/A, 12.04 lm/W, and 6.88%, and those of device R3 are 21008 cd/m^2, 10.08 cd/A, 10.20 lm/W, and 5.89%. Notably, R2 (0.8-wt% doping) achieves optimal performance, with EQE significantly exceeding the 5% theoretical limit for conventional fluorescent OLEDs.[33,34] An appropriate doping concentration is crucial for efficient FRET energy transfer. When the doping concentration of DCJTB is too low, the carrier injection efficiency and spatial distribution become less uniform,[35] and the emission sites of DCJTB are easily saturated by FRET energy transfer from PPIAn2N. These factors collectively lead to lower luminance and efficiency. Conversely, when the doping concentration increases to 1 wt% or higher, the intermolecular distance between PPIAn2N and DCJTB becomes small enough to fall within the Dexter transfer radius (0.5 nm–1 nm), triggering direct triplet energy transfer from PPIAn2N to DCJTB.[36] This process causes triplet excitons on DCJTB to relax nonradiatively to the ground state, resulting in significant exciton loss and a corresponding decline in device performance (see Fig. S4). A control device (RR) employing conventional host mCP (1,3-bis(N-carbazolyl)benzene) confirms PPIAn2N's superiority as a host material. With the structure: ITO/MoO_3 (3 nm)/TAPC (40 nm)/TCTA (10 nm)/mCP: DCJTB (0.8 wt%, 10 nm)/TmPyPB (40 nm)/LiF (1 nm)/Al (100 nm). Remarkably, devices R2 and R3 exhibited substantially higher luminance and efficiency compared to the reference device RR. In addition, all red devices R1–R3 display significantly reduced efficiency roll-off. The roll-off is 12.5%–23.5% at the luminance of 1000 cd/m^2, whereas the reference device RR suffers a severe efficiency roll-off of 54.7% at the same luminance level. These key performance parameters are summarized in Table 1.

Compared to the reference device RR employing the conventional host mCP, PPIAn2N-based devices R1–R3 exhibit outstanding EL performance. This enhancement is profoundly attributed partly to PPIAn2N's bipolar carrier transport property, which improves carrier recombination efficiency and broadens the recombination zone.[30] In addition, two different emission mechanisms are shown in Fig. 3. From Fig. 3(a), when HLCT PPIAn2N is employed as the host, because of the hot exciton mechanism, high-lying triplet excitons (T_n) can rapidly transfer energy to its singlet (S_1) through the hRISC process, which increases the proportion of singlet excitons on PPIAn2N.[22,37] It enables more singlet state excitons on PPIAn2N to transfer energy to DCJTB for emission, boosting luminance and device performance. However, in the mCP-hosted device as shown in Fig. 3(b), the injected hole and electron carriers form excitons on mCP. Only singlet excitons, accounting for 25% of the initially formed excitons, transfer energy to DCJTB for lighting through the FRET process, resulting in insufficient exciton utilization and lower performance.

To further validate the energy transfer mechanisms in these distinct doping systems, transient photoluminescence (PL) spectra of mCP and PPIAn2N films doped with 0.8-wt% DCJTB were measured. Fitting results confirm that PPIAn2N: DCJTB exhibits a significantly shorter emission lifetime (τ = 2.18 ns) than mCP: DCJTB (τ = 2.98 ns). According to the following formula:

$$\tau = \frac{1}{\kappa_{FET} + \kappa_r + \kappa_{nr}}, \tag{1}$$

where τ is the emission lifetime, κ_{FET} is the FRET rate, κ_r is the radiative rate, and κ_{nr} is the nonradiative rate. Clearly, τ and κ_{FET} are inversely related. The emission lifetime τ of PPIAn2N: DCJTB is shorter than that of mCP: DCJTB, indicating a more efficient energy transfer from PPIAn2N to DCJTB compared to mCP.[38,39] The above discussion out-

lines the fundamental physical mechanisms underlying the enhanced EL performance of PPIAn2N-based devices.

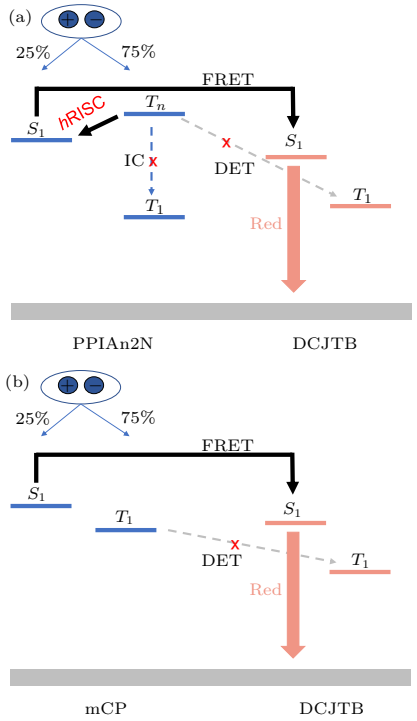

Fig. 3. Schematic emitting mechanism diagram for HLCT PPIAn2N (a) and mCP (b) hosted red devices with the doping concentration of DCJTB dopants ≤ 0.8 wt%. FRET: Forster energy transfer, DET: Dexter energy transfer; hRISC: Reverse intersystem crossing from high-lying triplet state (T_n, $n \geq 2$) to singlet state (S_1); IC: Internal conversion.

The above experimental results clearly demonstrate the feasibility of using the HLCT material PPIAn2N as a fluorescence-doped host. Motivated by these findings, in this paper, we further explore its potential as a host for the phosphorescent dopant in the following sections. Based on the above photophysical analysis, the phosphorescent emitter PO-01 is employed as a dopant to fabricate yellow OLEDs with the structure: ITO/MoO_3 (3 nm)/TAPC (40 nm)/TCTA (10 nm)/PPIAn2N: PO-01(x-wt%, 10 nm)/TmPyPB (40 nm)/LiF (1 nm)/Al (100 nm) ($x =$ 5, 8, and 12, corresponding to devices Y1, Y2, and Y3, respectively); the detailed device structure is shown in Fig. 4(a). As anticipated, the EL performance of devices Y1–Y3 exhibited a strong dependence on the doping concentration. As depicted in the EL spectra of Fig. 4(b), all devices successfully achieve yellow emission with an emission peak at approximately 573 nm. The J–V–L curves in Fig. 4(c) demonstrate that the fabricated OLEDs exhibit turn-on voltages as low as 2.4 V and reach a luminance of 10000 cd/m^2 at voltages of 4.2 V–4.8 V, which can be comparable to that based on p–i–n junctions.[40] Interestingly, as shown in Figs. 4(c)–4(e), the EL performance of devices Y1–Y3 first increases and then decreases with increasing PO-01 doping concentration. This behavior may result from inefficient energy transfer from PPIAn2N to PO-01 at lower concentrations, where the transfer efficiency is insufficient. At higher doping concentrations, the reduced intermolecular distance between PO-01 molecules leads to strong concentration quenching, causing significant non-radiative exciton loss and consequently compromised device performance.[41] Therefore, the optimal EL performance is achieved in device Y2 when 8 wt% of PO-01 is doped into the PPIAn2N and exhibits the maximum luminance of 93975 cd/m^2, CE of 63.65 cd/A, PE of 72.38 lm/W, and EQE of 25.08%. Notably, devices Y1–Y3 exhibit negligible efficiency roll-off at a practical luminance of 1000 cd/m^2. These key performance parameters are summarized in Table 1. Such excellent luminescent properties are attributed to the high and balanced hole and electron mobility of PPIAn2N, which promotes efficient carrier transport and broadens the exciton recombination zone.[22] In addition, as shown in Fig. S5, the EL characteristics of the reference device YR (mCP: 8-wt% PO-01) are evaluated. Device Y2 exhibits superior EL performance compared with YR, suggesting that the triplet excitons of PO-01 are efficiently confined within the HLCT host and suffer negligible quenching, which facilitates FRET energy transfer from PPIAn2N to the PO-01 dopant, facilitates the hRISC (T_n–S_1) process, and reduces the accumulation of triplet excitons on PPIAn2N significantly (Fig. 5(a)). This suppression of triplet–triplet annihilation (TTA) and triplet–polaron quenching (TPQ) is a key factor enabling the device to maintain a high EQE even at high luminance.[42] Meanwhile, as shown in Figs. 4(f) and S6, all devices exhibit stable yellow emission. Specifically, device Y2 shows CIE coordinates of (0.533, 0.459) at an applied voltage of 5 V. These results collectively demonstrate that PPIAn2N is an excellent host material for the yellow phosphorescent PO-01. Some representative Ph-OLEDs based on PO-01 are shown in Table S1.

The charge carrier trapping and energy transfer are two important mechanisms in doped OLEDs.[43] The charge carrier trapping behavior of the guest molecule PO-01 is evaluated based on the analysis of the energy levels of the HOMO/LUMO, which shows that PO-01 has an LUMO level similar to that of PPIAn2N, but a significantly shallower HOMO level, suggesting the presence of a hole trapping effect. The single-carrier devices are fabricated with the following structures: ITO/MoO_3 (3 nm)/TAPC (40 nm)/EML (10 nm)/TAPC (40 nm)/Al (100 nm) for hole-only devices (H1 and H2) and ITO/TmPyPB (40 nm)/EML (10 nm)/TmPyPB (40 nm)/LiF (1 nm)/Al (100 nm) for electron-only devices (E1 and E2). The EML consists of PPIAn2N or PPIAn2N:8 wt% PO-01. As evident from the J–V curves in Figs. S7(a) and S7(b), device H2 exhibits lower current density than H1, whereas E1 and E2 demonstrate comparable current densities, which indicates that PO-01 exhibits a more pronounced hole trapping effect. These findings provide an important foundation for the structural design of high-performance dual-EML white OLEDs.

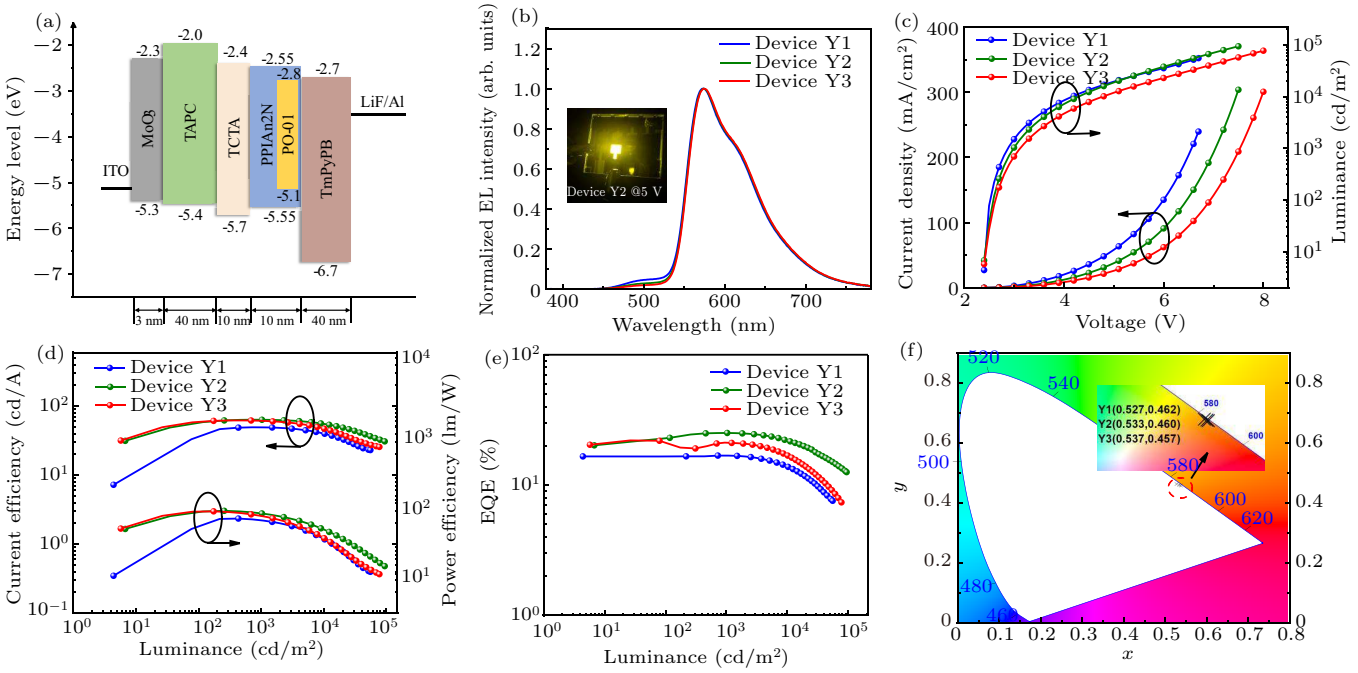

Fig. 4. (a) Schematic device structure and energy level diagram for yellow devices, (b) normalized EL spectra for yellow devices at 5 V, (c) *J*–*V*–*L* curves; (d) CE–L–PE curves, (e) EQE–L curves, (f) CIE coordinates of yellow devices Y1–Y3 at 5 V.

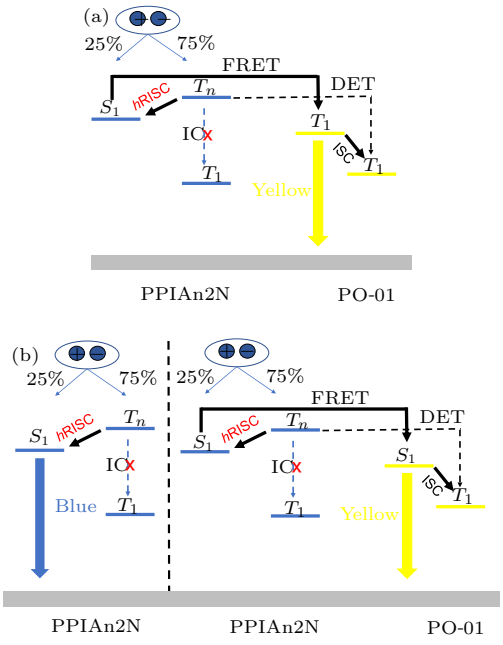

Fig. 5. Working mechanisms of the resulting yellow OLED and dual-EML hybrid WOLED.

As for the complementary two-color white OLEDs, it requires the synergistic luminescence from PPIAn2N and PO-01 to cover the whole visible region as much as possible. The spectral complementarity between the PPIAn2N-based blue device and the aforementioned yellow device, with their CIE coordinates just connecting across the white region (see Figs. S8(a)–S8(b)), demonstrates the feasibility of developing high color quality two-color white OLEDs.[44,45] Therefore, incorporating a blue-emitting layer alongside the existing yellow-phosphorescent structure enables straightforward fabrication of dual-EML white OLEDs with yellow/blue complementary emission. Compared to single-EML WOLEDs, the dual-EML architecture offers significant advantages, including enhanced flexibility in layer configuration and precise control over charge and exciton distribution. These advantages enable a highly promising pathway toward high-performance hybrid WOLEDs with low efficiency roll-off through the full utilization of both singlet and triplet excitons.[10] To mitigate the impact of the hole trapping effect, a series of two-color white OLEDs are strategically designed with the following structure: ITO/MoO_3 (3 nm)/TAPC (40 nm)/TCTA (10 nm)/PPIAn2N (x nm)/PPIAn2N: PO-01 (8 wt%, 10 nm)/TmPyPB (40 nm)/LiF (1 nm)/Al (100 nm), where $x = 5$, 10, and 15 nm correspond to devices W1, W2, and W3. Varying the x value is intended to adjust the intensity of blue emission to achieve balanced white emission. The complementary emitting mechanism and detailed device structure are illustrated in Figs. 5(b) and 6(a).

As anticipated, all devices in Fig. 6(b) exhibit white light emission with two wavebands corresponding to the intrinsic emissions of PPIAn2N and PO-01. The significantly stronger yellow emission intensity relative to blue indicates predominant confinement of the exciton recombination zone within the yellow-emitting layer. As shown in Fig. 6(c) and Table 2, devices W1–W3 exhibit higher turn-on voltages than the aforementioned yellow devices. This is attributed to the introduction of additional carrier injection barriers caused by the incorporation of the blue layer. As the thickness of the blue layer PPIAn2N increases from 5 nm to 15 nm, the device efficiency gradually decreases. W1 shows the maximum luminance of 74098 cd/m^2, CE of 38.67 cd/A, PE of 39.90 lm/W, and EQE of 17.03%. W2 delivers 43685 cd/m^2, 24.17 cd/A,

26.65 lm/W, and 10.79%, while W3 shows 39575 cd/m^2, 15.10 cd/A, 13.77 lm/W, and 7.11%. W1 demonstrates optimal EL performance, maintaining a high EQE of 15.82% at 1000 cd/m^2 with merely 7.1% efficiency roll-off (Figs. 6(c)–6(e)). This results from a slight anode-ward shift of the exciton recombination zone with increasing blue-layer thickness, which elevates the electron–hole recombination probability in the blue-emitting layer, thereby enhancing blue emission. However, due to the intrinsic efficiency limitations of the PPIAn2N-based blue device, more excitons emit in the blue layer but are wasted, which leads to a decline in white device performance.[29] For comparison, a white reference device (WR) with inverted layer sequence: ITO/MoO_3 (3 nm)/TAPC (40 nm)/TCTA (10 nm)/PPIAn2N: PO-01 (8 wt%, 10 nm)/PPIAn2N (10 nm)/TmPyPB (40 nm)/LiF (1 nm)/Al (100 nm) is fabricated, where the blue-emitting layer is positioned adjacent to the electron-transport layer.

As shown in Table 2, device WR exhibits a maximum CE of 16.51 cd/A, a PE of 14.32 lm/W, and an EQE of 7.75%, respectively, which are significantly lower than those of W2. Due to the strategic positioning of the hole-trapping layer away from the hole injection side, which partially mitigates the hole trapping effect of PO-01 and prevents excessive hole aggregation in the yellow-emitting layer. Consequently, balanced carrier transport is achieved within the dual-emission layers, highlighting the crucial role of precise emission layer tuning in developing high-performance HLCT-WOLEDs. As evidenced by Figs. 6(f)–6(i) and S7, all devices exhibit stable warm white emission, highlighting their significant potential as health-compatible light sources.[46] Crucially, Device W1 maintains exceptional color stability under high-luminance conditions with minimal CIE coordinate shifts of (0.005, 0.005) as the driving voltage increases from 7 V to 9 V. This performance matches that of three-color white OLEDs reported in the literature,[47,48] demonstrating promising application prospects. Notably, such stable white emission at high brightness is one of the notable outcomes among recently reported hybrid white OLEDs (Table S2). These results confirm the feasibility and advantages of simultaneously employing an HLCT material as both the blue emitter and the host for the phosphorescent dopant in the complementary long-wavelength for white OLED development.

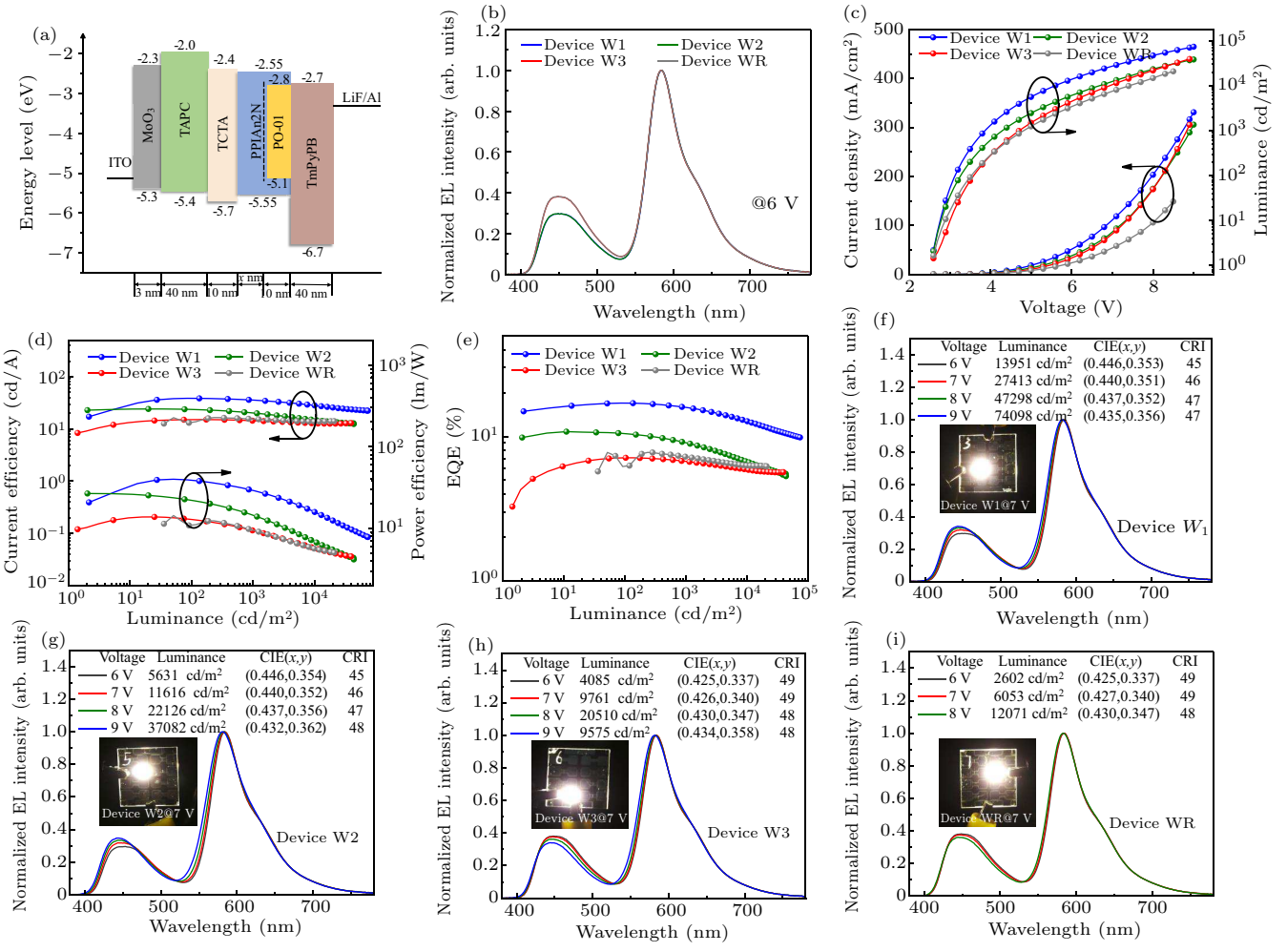

Fig. 6. (a) Schematic device structure and energy level diagram for white devices W1–WR, (b) normalized EL spectra for white devices W1–WR at 6 V, (c) *J*–*V*–*L* curves, (d) CE–L–PE curves, (e) EQE–L curves, (f)–(h) normalized EL spectra, luminance, CIE coordinates, and CRI for W1–W3 at 6 V–9 V, (i) corresponding results for WR at 6 V–8 V.

Table 2. Summary of key performance parameters for white devices in this work.

Device	V_{on} (V)	L_{max} (cd/m^2)	CE (cd/A)/PE (lm/W)/EQE (%)		CIE(x,y)	Roll off (%)	CRI
			Maximum	At 1000 cd/m^2			
W1	2.6	74098	38.67/39.90/17.03	35.62/28.69/15.82	(0.440,0.351)	7.1	47
W2	2.6	43685	24.17/26.65/10.79	20.23/14.44/9.03	(0.440,0.352)	16.3	47
W3	2.7	39575	15.10/13.77/7.11	14.39/9.42/6.72	(0.426,0.340)	5.5	48
WR	2.9	20992	16.51/14.32/7.75	15.51/9.55/7.24	(0.427,0.340)	6.6	49

V_{on}: the voltage at the luminance of 1 cd/m^2; L_{max}: the maximum luminance of the devices; CIE(x,y): CIE coordinates obtained at a voltage of 7 V; Roll off: roll off value = (maximum EQE – EQE@1000 cd/m^2)/maximum EQE. CRI: CRI obtained at a voltage of 8 V.

3. Conclusion and perspectives

In this work, the blue emission PPIAn2N with HLCT excited state and bipolar carrier transport properties is employed as a sensitizing host. By precisely controlling the doping concentration, high-performance red fluorescent and yellow phosphorescent OLEDs based on DCJTB and PO-01 are successfully fabricated, achieving maximum EQEs of 6.88% and 25.08%, respectively. The yellow phosphorescent device shows negligible efficiency roll-off, attributed to enhanced FRET energy transfer from PPIAn2N to PO-01 facilitated by the *h*RISC process. On this basis, PPIAn2N is further utilized as both the blue emitter and the sensitizing host for PO-01 to construct a fluorescent/phosphorescent hybrid white OLED through rational dual-EML structure arrangement. The resulting white device obtains ideal white emission with a maximum CE of 38.67 cd/A, PE of 39.90 lm/W, EQE of 17.03%, and luminance of 74098 cd/m^2. Notably, the CIE coordinates remain highly stable with a variation of only (0.005, 0.005) under driving voltages from 7 V to 9 V, demonstrating huge potential for practical applications. This work not only further confirms the feasibility of using HLCT materials simultaneously as host and emitter for both monochrome and white OLEDs, but also offers a new strategy for the development of high-performance doped OLEDs.

Acknowledgements

Project supported by the National Key Research and Development Program of China (Grant No. 2022YFB3603002), the Regional Joint Fund of the National Natural Science Foundation of China (Grant Nos. U21A20492 and 62275041), the Sichuan Province Science and Technology Program (Grant No. 2023ZDZX0020), the Natural Science Foundation Youth Program of Sichuan Province, China (Grant No. 2025ZNSFSC1421), and the Sichuan Province Key Laboratory of Display Science and Technology and the Qiantang Science & Technology Innovation Center.

References

[1] Tang C W and VanSlyke S A 1987 *Appl. Phys. Lett.* **51** 913
[2] Hong G, Gan X, Leonhardt C, Zhang Z, Seibert J, Busch J M and Bräse S 2021 *Adv. Mater.* **33** 2005630
[3] Song J, Lee H, Jeong E G, Choi K C and Yoo S 2020 *Adv. Mater.* **32** 1907539
[4] Chen H W, Lee J H, Lin B Y, Chen S and Wu S T 2017 *Light: Science & Applications* **7** 17168
[5] Reineke S, Lindner F, Schwartz G, Seidler N, Walzer K, Lüssem B and Leo K 2009 *Nature* **459** 234
[6] D'Andrade B W and Forrest S R 2004 *Adv. Mater.* **16** 1585
[7] Huang F C, Sun X D, Shi Y and Pan L J 2024 *Soft Sci.* **4** 40
[8] Lee J H, Chen C H, Lee P H, Lin H Y, Leung M K, Chiu T L and Lin C F 2019 *J. Mater. Chem. C* **7** 5874
[9] Im Y, Byun S Y, Kim J H, Lee D R, Oh C S, Yook K S and Lee J Y 2017 *Adv. Funct. Mater.* **27** 1603007
[10] Wu Z and Ma D 2016 *Materials Science and Engineering: R: Reports* **107** 1
[11] Jankus V, Chiang C J, Dias F and Monkman A P 2012 *Adv. Mater.* **25** 1455
[12] Ahn D H, Kim S W, Lee H, Ko I J, Karthik D, Lee J Y and Kwon J H 2019 *Nat. Photon.* **13** 540
[13] Beljonne D, Ye A, Shuai Z and Brédas J L 2004 *Adv. Funct. Mater.* **14** 684
[14] Wu C J, Zhu H, Wang X, Yuan W N, Tian Y L, Jiang X C, Han Y T, Gao X Q and Lai W Y 2025 *Soft Sci.* **5** 42
[15] Wu C, Shi K, Li S, Yan J, Feng Z Q, Tong K N, Zhang S W, Zhang Y, Zhang D, Liao L S, Chi Y, Wei G and Kang F 2024 *EnergyChem* **6** 100120
[16] Sun J, Ahn H, Kang S, Ko S B, Song D, Um H A, Kim S, Lee Y, Jeon P, Hwang S H, You Y, Chu C and Kim S 2022 *Nat. Photon.* **16** 212
[17] Li G, Fleetham T, Turner E, Hang X C and Li J 2014 *Adv. Opt. Mater.* **3** 390
[18] Cai X and Su S J 2018 *Adv. Funct. Mater.* **28** 1802558
[19] Li W, Pan Y, Xiao R, Peng Q, Zhang S, Ma D, Li F, Shen F, Wang Y, Yang B and Ma Y 2013 *Adv. Funct. Mater.* **24** 1609
[20] Li W, Pan Y, Yao L, Liu H, Zhang S, Wang C, Shen F, Lu P, Yang B and Ma Y 2014 *Adv. Opt. Mater.* **2** 892
[21] Luo Q, Gao Y, Bai Y, Wu M, Xu H, Wang H, Zheng D and Yu J 2024 *Adv. Opt. Mater.* **13** 2402881
[22] Luo Q, Gao Y, Xu H, Zhao S, Dong W, Miao Y, Wang Y, Wang H and Yu J 2023 *J. Mater. Chem. C* **11** 15918
[23] Xu Y, Xu P, Hu D and Ma Y 2020 *Chem. Soc. Rev.* **50** 1030
[24] Xue S, Qiu X, Ying S, Lu Y, Pan Y, Sun Q, Gu C and Yang W 2017 *Adv. Opt. Mater.* **5** 1700747
[25] Zhao F and Ma D 2017 *Materials Chemical Frontiers* **1** 1933
[26] Ma W, Bin Z, Yang G, Liu J and You J 2022 *Angew. Chem. Int. Ed.* **61** e202116681
[27] Yang J, Zheng W, Hu D, Zhu F, Ma Y and Yan D 2022 *Adv. Sci.* **10** 2203997
[28] Liu H, Liu F, Cheng Z, Yan Y, Wan L, Hu Y, Xu Y, Ma X and Lu P 2024 *Adv. Opt. Mater.* **12** 2401424
[29] Li X, Wang X, Xu H, Zhao B, Guo Y, Miao Y, Liu B, Yue G and Wang H 2024 *Chem. Eng. J.* **485** 150064
[30] Zhao B, Miao Y, Wang Z, Wang K, Wang H, Hao Y, Xu B and Li W 2016 *Nanophotonics* **6** 1133
[31] Sahoo H 2011 *Journal of Photochemistry and Photobiology C: Photochemistry Reviews* **12** 20
[32] Chen P, Xiong Z, Peng Q, Bai J, Zhang S and Li F 2014 *Adv. Opt. Mater.* **2** 142
[33] Tao Y, Yuan K, Chen T, Xu P, Li H, Chen R, Zheng C, Zhang L and Huang W 2014 *Adv. Mater.* **26** 7931
[34] Cao Y, Parker I D, Yu G, Zhang C and Heeger A J 1999 *Nature* **397** 414
[35] Tian Q S, Yuan S, Shen W S, Zhang Y L, Wang X Q, Kong F C and Liao L S 2020 *Adv. Opt. Mater.* **8** 2000556

[36] Chen J X, Wang K, Xiao Y F, Cao C, Tan J H, Wang H, Fan X C, Yu J, Geng F X, Zhang X H and Lee C S 2021 *Adv. Funct. Mater.* **31** 2101647
[37] Guo K, Lin C, Wu Y, Xiao S, Qiao X, Yang D, Dai Y, Sun Q, Chen J, Hu D, Ying L, Ma Y and Ma D 2023 *Adv. Opt. Mater.* **11** 2202988
[38] Li X Y, Wu Z R, Chen Z T and Shi J D 2025 *Soft Sci.* **5** 16
[39] Keum K, Yang S, Kim K S, Park S K and Kim Y H 2024 *Soft Sci.* **4** 34
[40] Wu Z, Yu L, Zhao F, Qiao X, Chen J, Ni F, Yang C, Ahamad T, Alshehri S M and Ma D 2017 *Adv. Opt. Mater.* **5** 1700415
[41] Zou S H, Li Y Z and Gong Z 2024 *Soft Sci.* **4** 19
[42] Lin C, Han P, Xiao S, Qu F, Yao J, Qiao X, Yang D, Dai Y, Sun Q, Hu D, Qin A, Ma Y, Tang B Z and Ma D 2021 *Adv. Funct. Mater.* **31** 2106912
[43] Yu Y, Wang R, Chao X, Li T, Xie M, Ying S, Sun Q, Pan Y, Xue S and Yang W 2022 *Chem. Eng. J.* **441** 136048
[44] Zhang J, Han C, Du F, Duan C, Wei Y and Xu H 2020 *Adv. Funct. Mater.* **30** 2005165
[45] Tang X, Liu X Y, Jiang Z Q, Liao L S 2019 *Adv. Funct. Mater.* **29** 1807541
[46] Liu H, Tang X, Cheng Z, Hu Y, Yan Y, Xu Y, Su Z, Liu F and Lu P 2024 *Chin. Chem. Lett.* **35** 109809
[47] Zhang H, Xue J, Li C, Zhang S, Yang B, Liu Y and Wang Y 2021 *Adv. Funct. Mater.* **31** 2100704
[48] Liu H, Fu Y, Tang B Z and Zhao Z 2023 *Adv. Funct. Mater.* **33** 2309770